Spin bias: theory and observations

A.D. Montero-Dorta[1,2]

[1] *Departamento de Física, Universidad Técnica Federico Santa María, Chile*
[2] *Departamento de Física Matemática, Instituto de Física, Universidade de São Paulo, Brasil*

Contact / amonterodorta@gmail.com

Resumen / Resumo aquí mi contribución a la 62a Reunión de la Asociación Argentina de Astronomía. Mi presentación se centró en la conexión halo-galaxia y, en particular, en el fenómeno conocido como *secondary halo bias*. Este término engloba todas las dependencias secundarias (a masa de halo fija) de la distribución espacial de los halos. El presente artículo aborda una de estas dependencias, el llamado *halo spin bias*, que corresponde a la contribución del spin al agrupamiento o *clustering* de los halos. Muestro aquí una medida precisa del efecto, discuto algunos de los mecanismos físicos asociados con el mismo y propongo un posible método de observación basado en el efecto Sunyaev-Zel'dovich.

Abstract / I summarize here my contribution to the 62a Meeting of the Argentinian Astronomical Society. My presentation addressed the halo-galaxy connection and, in particular, the effect called *secondary halo bias*, which refers to the secondary dependencies of halo clustering at fixed halo mass. In this paper, I focused on one of these secondary dependencies, the so-called *halo spin bias*, which corresponds to the contribution from halo spin. I show here a high signal-to-noise measurement of the effect, discuss some of the physical mechanisms associated with it, and propose a method to probe it with future observations based on the Sunyaev-Zel'dovich effect.

Keywords / cosmology: theory — dark matter — large-scale structure of universe — galaxies: halos

1. Introduction

Linear halo bias describes the relation between the density contrast of dark-matter (DM) halos and that of the underlying matter density field, i.e, $b = \delta_{\rm h}/\delta_{\rm m}$. Although halo bias is known to be stochastic and scale-dependent, it is common to assume that this quantity depends exclusively on halo mass on sufficiently large scales, i.e., $b(M_{\rm vir})$. This assumption is well founded in the context of physically-motivated analytical models of hierarchical clustering such as the Press-Schechter formalism (Press & Schechter, 1974) and the peak-background split model (Sheth & Tormen, 1999).

However, since the seminal works of Sheth & Tormen (2004) and Gao et al. (2005), the existence of secondary dependencies for halo clustering, $b(X|M_{\rm vir})$, has become progressively more evident. In fact, today we know that virtually any given internal halo property, X, displays a certain level of secondary bias, with the corresponding mass trend depending strongly on the halo property under analysis (see, e.g., Sheth & Tormen 2004; Gao et al. 2005; Wechsler et al. 2006; Gao & White 2007; Dalal et al. 2008; Salcedo et al. 2018; Sato-Polito et al. 2019; Johnson et al. 2019; Mansfield & Kravtsov 2020; Tucci et al. 2021, to name just a few).

Among the different dependencies that can be measured in N-body numerical simulations, only recently has some attention been given to the dependence on halo spin, λ (even though this contribution was already measured in the early works). Halo spin is commonly defined in simulations as a dimensionless parameter proportional to the total angular momentum of the DM particles (Peebles, 1969; Bullock et al., 2001), namely:

$$\lambda = \frac{|J|}{\sqrt{2}\, M_{\rm vir} V_{\rm vir} R_{\rm vir}}, \qquad (1)$$

for the Bullock et al. version, where J is the halo angular momentum inside a sphere of radius $R_{\rm vir}$ and mass $M_{\rm vir}$ and $V_{\rm vir}$ is its circular velocity at virial radius $R_{\rm vir}$.

The so called "spin bias" effect (e.g., Gao & White 2007; Sato-Polito et al. 2019; Johnson et al. 2019; Tucci et al. 2021), $b(\lambda|M_{\rm vir})$, can be divided into two regimes. At the low-mass end, lower-spin halos are more tightly clustered than higher-spin halos of the same mass, due to the effect of splashback halos (Tucci et al., 2021). At the high-mass end, the opposite trend is observed and the physical mechanisms responsible for it are yet to be established. It appears, however, that this "intrinsic" dependence could be related to fundamental theories that link the angular momentum of halos to the tidal field (e.g. Barnes & Efstathiou 1987).

Elucidating the physical origins of the multiple manifestations of secondary bias and their effect on the "baryonic sector" is key to our understanding and modelling of the halo-galaxy connection in the physical context of the large-scale structure (LSS) of the Universe (see a review in Wechsler & Tinker 2018). Characterizing this link with precision is in turn of paramount importance for the extraction of cosmological information from upcoming galaxy data sets. This short paper is based on my contribution as an invited speaker at the *62a Reunión de la Asociación Argentina de Astronomía*, where I summarized results from several recent spin-bias works. The paper is organized as follows. Section 2 describes the basic method to measure halo spin bias from

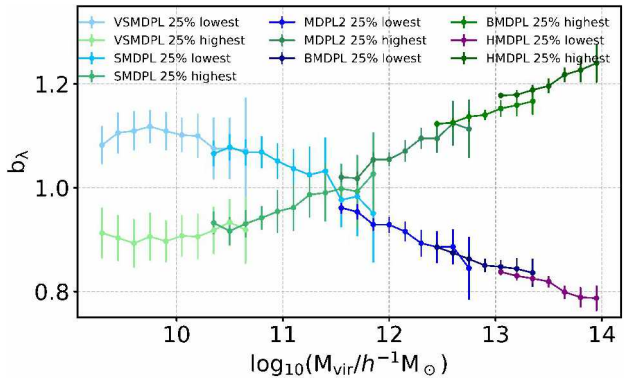

Figure 1: The halo spin bias measurement from the MultiDark suite of N-body numerical simulations at $z = 0$. Each point represents the relative bias between the high-spin (greener colors) or the low-spin (bluer colors) quartiles and the entire population at a given halo mass bin. Error bars show the standard deviation computed from a set of sub-boxes. The MultiDark boxes employed are distinguished by progressively darker tones. From left to right, results from the Very Small MultiDark (VSMD), Small MultiDark (SMD), MultiDark Plack 2 (MDPL2), Big MultiDark (BMD) and Huge MultiDark (HMD) boxes are shown.

simulations and discusses the physical origins of the effect. Section 3 addresses the manifestation of spin bias on the galaxy population from hydrodynamical simulations. Section 4 is devoted to the detectability of the effect in observations. The main conclusions of this series of papers are succinctly summarized in Sec. 5.

2. Halo spin bias: a particular case of secondary halo bias

2.1. Measurement

The secondary dependencies of halo clustering are usually measured in N-body numerical simulations in terms of the relative bias of subsets of halos at fixed halo mass. In its simplest form, for a property X, the relative bias between the high-X subset and the entire i-th mass bin (M_i) can be simply computed from the ratio of the auto-correlation functions:

$$b_{\mathrm{X,high}}{}^2 = \frac{\xi_{[\mathrm{X_{high}},\mathrm{X_{high}}]}}{\xi_{[M_i,M_i]}}. \quad (2)$$

If, similarly, the relative bias for the low-X population, $b_{\mathrm{X,low}}$, is measured, the secondary-bias signal can be defined by comparing the two values. Importantly, secondary bias is usually measured by averaging over a range of scales around 5-15 h^{-1} Mpc, although the effect is known to be scale-dependent (see, e.g. Gao et al. 2005; Sunayama et al. 2016). In order to maximise the signal, the subsets are usually built as quartiles enclosing the 25% higher- (lower-) X-property population. It is also common to use definitions of halo bias based on the cross-correlations between subsets, which tend to increase the signal-to-noise of the measurements (see, e.g., Sato-Polito et al. 2019; Montero-Dorta et al. 2020b; Tucci et al. 2021).

In Sato-Polito et al. (2019), we provide one of the most precise measurements of secondary halo bias available in the literature, combining multiple state-of-the-art MultiDark* N-body simulation boxes in order to increase the mass coverage. Three of the main secondary halo properties are addressed in the aforementioned analysis: age (parametrized in terms of $a_{1/2}$, the scale factor at which the halo accretes half of its mass), concentration (c_{200}, see Klypin et al. 2011), and spin (λ, see Bullock et al. 2001). Different internal halo properties display different signals, with the age dependence, usually called "halo assembly bias", being the most notorious one. At the low-mass end, halos that assemble their mass earlier are significantly more clustered than halos that form at later times.

The physical origins of low-mass assembly bias are still not fully established, although several theories have attempted to relate the effect with the truncation of mass accretion in a subpopulation of halos. This "stalled evolution" could be caused by tidal interactions with a nearby halo (e.g., Dalal et al. 2008; Salcedo et al. 2018) or by the global tidal fields (e.g., Borzyszkowski et al. 2017; Musso et al. 2018; Ramakrishnan et al. 2019).

The secondary dependence of halo bias on spin, the main focus of this paper, is shown in Fig. 1. This figure clearly indicates the two regimes that spin bias can be divided into, delimited by a characteristic mass $\log_{10}(M_{\mathrm{vir}}/h^{-1}\mathrm{M}_\odot) \simeq 11.5$ at $z = 0$. In the next section, I will show how the inversion of the signal at the low-mass end is caused by the effect of splashback halos.

2.2. Physical origins

It is important to establish that the different secondary bias trends are not mutually independent, since halo properties typically correlate with each other. As an example, older halos tend to be more concentrated, while younger halos have typically larger spin parameters. Importantly, this does not imply either that all secondary bias trends emanate from the same common mechanism, as several physical processes have been shown to produce a certain amount of signal (see, e.g., Dalal et al. 2008; Borzyszkowski et al. 2017; Mansfield & Kravtsov 2020; Tucci et al. 2021).

In Tucci et al. (2021), we show that the inverted spin bias signal at the low-mass end is caused by a particular population of halos called "splashback halos". The splashbacks are distinct halos at the redshift under analysis that were subhalos at previous times, as they passed through the virial radius of a more massive halo. The effect of splashbacks as a function of redshift is shown in Fig. 2. The upper panel of this figure displays the spin bias measurement in different redshift snapshots up to $z = 1.5$. Notably, the characteristic inversion (or "crossover") mass moves to lower masses as redshift increases (vanishing outside our mass range at $z > 1$), as expected from the evolution of the height of the density peaks. The lower panel shows the effect of removing splahsbacks from the simulation: the inversion

*http://skiesanduniverses.org

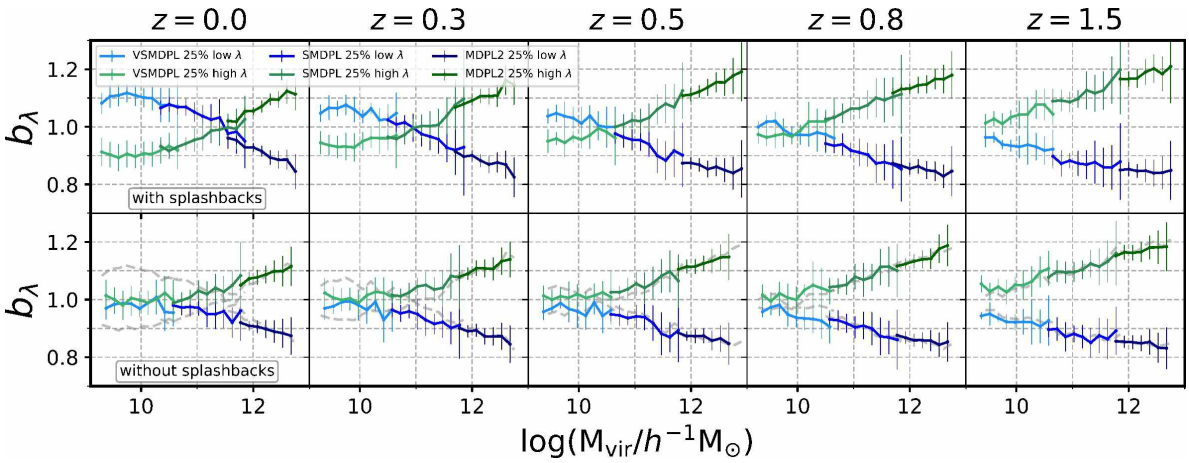

Figure 2: Redshift dependence of halo spin bias and the effect of splashback halos measured from a set of MultiDark N-body simulation boxes (VSMD, SMD, MDPL2). *Upper row:* the original signal for the entire sample. *Lower row:* the "intrinsic" signal once splashbacks are removed from the sample (the original, uncorrected signal is also shown in a dashed line). Error bars correspond to the box-to-box standard deviation of the measurement.

disappears in all snapshots and a consistent behaviour where higher-λ halos are more tightly clustered than their lower-λ counterparts is recovered throughout the mass range considered.

The dramatic impact of splashbacks can be understood from their location in the LSS. They live in the vicinity of very massive halos, so their large-scale bias is determined by their massive neighbors. Essentially, more massive halos are more biased, as expected from the primary dependence of halo clustering, which in turn explains the high bias of splashbacks (despite their low masses). The second piece of the puzzle comes from the fact that splashbacks have typically low spin parameters, which, as in the case of subbhalos, seems to be a consequence of the strong tidal forces that they experience (see discussion in Lee et al. 2018; Tucci et al. 2021). Since the effect of splashbacks on spin bias is indirectly caused by other (more massive) halos, it can be considered a contamination of the intrinsic signal. It is possible, in fact, that the recently proposed definition of the halo boundary based on the "splashback radius" (see, e.g., Diemer 2020) could naturally eliminate this contribution.

The above results clarify the spin bias picture at the low-mass end. However, the physical origins of the intrinsic (mostly high-mass) signal are still unclear. Theoretical works point towards the tidal torque theory (TTT, Barnes & Efstathiou 1987; Heavens & Peacock 1988), in which the angular momentum is induced by the misalignment between the large-scale tidal field and the inertia tensor. Since the tidal field is expected to be stronger in highly-biased large-scale environments, this connection could potentially explain the larger bias of higher-spin halos at the high mass end (see Tucci et al. 2021 for more discussion). It seems promising therefore to establish a theoretical link between the seminal TTT theory and recent physical interpretations of assembly bias based on the effect of (isotropic vs. anisotropic) tidal environments (e.g., Borzyszkowski et al. 2017; Musso et al. 2018; Ramakrishnan et al. 2019).

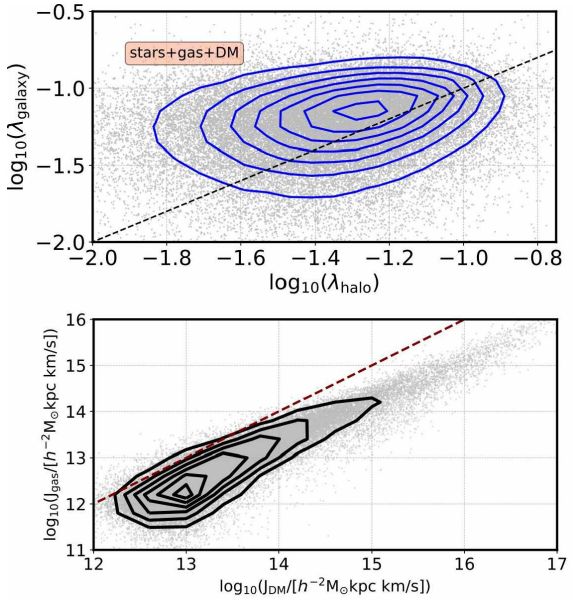

Figure 3: *Upper panel:* The correlation between total galaxy spin (including stars, gas, and DM) and total halo spin in IllustrisTNG300. *Lower panel:* In the same simulation, the correlation between the angular momentum of the intra-halo gas and the angular momentum of the DM component. The one-to-one relation is marked by a dashed line.

3. The manifestation of halo spin bias on the galaxy population

So far we have only addressed the connection between an internal halo property (spin) and halo bias. Hydrodynamical simulations allow us to go a step further and investigate the multiple potential manifestations of secondary halo bias on the galaxy population, a link that

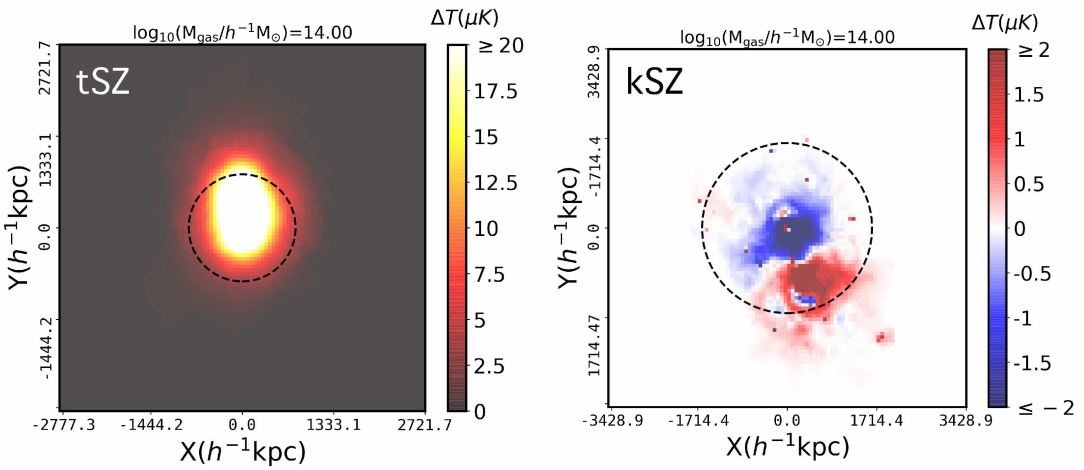

Figure 4: *Left panel*: A tSZ map for a randomly chosen halo containing a total gas mass of $\log_{10}(M_{\rm gas}/h^{-1}M_\odot) = 14$ in IllustrisTNG300. Each pixel shows the tSZ temperature distorsions induced on the CMB, $[\Delta T]_{\rm tSZ}$, in units of μK, assuming $T_{\rm CMB} = 2.725$ K. The halo-centric circle indicates the region where 2/3 of gas particles reside. In order to show the tSZ substructure of the halos, a saturation limit at $[\Delta T]_{\rm tSZ} = \pm 20$ μK is set on the color bar. *Right panel:* The kSZ map for the same halo after subtraction of group velocity, displaying the dipole structure. A saturation limit of $[\Delta T]_{\rm kSZ} = \pm 2$ μK is set on the color bar. In both cases, the line of sight is assumed to lie perpendicular to the total rotation axis of the halo.

has been hard to establish with observations. These hypothetical effects are generally referred to as "galaxy assembly bias" in the literature, by analogy with the halo assembly bias terminology. Note that galaxy assembly bias can be understood as a direct manifestation of secondary halo bias, i.e., the dependence of galaxy clustering on halo properties at fixed halo mass (see, e.g., Lin et al. 2016; Montero-Dorta et al. 2017). It can also be viewed from the perspective of halo occupations, as the dependence of the galaxy content of halos ("occupancy variations") on halo properties beyond halo mass (see, e.g., Salcedo et al. 2020).

In Montero-Dorta et al. (2020b), we use the IllustrisTNG300 magneto-hydrodynamical simulation (Pillepich et al. 2018) to investigate the galaxy clustering effect. In the context of spin bias, we show that total galaxy spin (including the contributions from stars, gas and DM, $\lambda_{\rm galaxy}$) is correlated with the total spin of the hosting halos (upper panel of Fig. 3). However, this correlation almost vanishes completely when the stellar spin ($\lambda_{\rm stellar}$) is chosen. Despite this diverse level of correlation, the underlying halo spin bias trend is surprisingly recovered when the central galaxy population is split by either spin value, at fixed halo mass. This result deserves further investigation (see Montero-Dorta et al. 2020b for details).

The analysis of IllustrisTNG300 yields another interesting result that motivates the study presented in the following section. In the lower panel of Figure 3, the angular momentum of the intra-cluster gas (defined here as all the gas and stars inside halos, including galaxies) is shown as a function of the angular momentum of the DM component. This figure demonstrate that, although the different physical processes that take place inside halos contribute to the turbulent motion of the gas, the rotation of this component is still tightly linked to that of DM. This correlation opens the door for the potential observational probe of halo spin bias that I describe in the following section.

4. Probing halo spin bias with observations: the SZ effect

Figure 3 suggests that measuring the rotation of the intra-cluster gas could provide a means of determining (DM/total) halo spin, which could in turn lead to an observational test for spin bias. The intra-cluster gas can be probed using the Sunyaev-Zel'dovich effect (SZ, Sunyaev & Zel'dovich 1970 and thereafter). The SZ effect consists of the inverse Compton scattering of photons from the Cosmic Microwave Background (CMB) as they propagate through galaxy clusters. This process produces two main types of temperature distortions on the CMB that can be measured with the right instrumentation:

- Thermal SZ (tSZ) effect: The scattering of CMB photons is due to the random, thermal motion of electrons inside clusters. This is the leading effect and the associated temperature distortions can be estimated as:

$$y(\mathbf{n}) \equiv \frac{\sigma_{\rm T} k_B}{m_{\rm e} c^2} \int_{\rm los} dl\ T_{\rm e}\ n_{\rm e}, \tag{3}$$

$$\left[\frac{\Delta T}{T_{\rm CMB}}\right]_{\rm tSZ}(\mathbf{n}) = g(x) y(\mathbf{n}) \tag{4}$$

where y is the "Compton parameter", $\mathbf{n}$ is the unit vector that defines the line of sight (los), $\sigma_{\rm T}$ is the Thomson cross-section, k_B is the Boltzmann's constant, $T_{\rm e}$ is the electron temperature, $m_{\rm e}$ is the electron rest mass, c is the speed of light, and $n_{\rm e}$ is the electron number density. The temperature distorsions $[\Delta T/T_{\rm CMB}]_{\rm tSZ}$ are equal to the Compton parameter times a conversion factor $g(x)$ at a given dimensionless frequency $x \equiv h\nu/(k_B T)$.

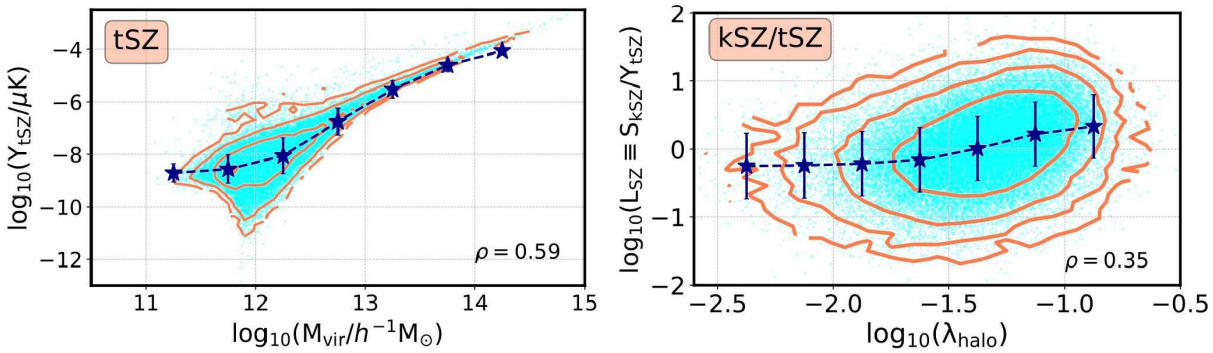

Figure 5: *Left panel:* The correlation between the integrated tSZ signal, $Y_{\rm tSZ}$ and the halo mass for the entire IllustrisTNG300 halo sample. *Right panel:* The correlation between the ratio of the integrated kSZ and tSZ signals, $L_{\rm SZ}$, and total halo spin, for the same sample. In both panels, the median values of the signals and corresponding standard deviations are overplotted. The Spearman rank-order correlation coefficients, ρ, are also included for reference.

- Kinetic SZ (kSZ) effect: The scattering of CMB photons is produced by the bulk motion of electrons inside clusters, which induces a Doppler shift. The kSZ temperature distortions are in this case:

$$\left[\frac{\Delta T}{T_{\rm CMB}}\right]_{\rm kSZ}(\mathbf{n}) = \frac{\sigma_T}{c}\int_{\rm los} dl\ n_{\rm e}\ \mathbf{v}\ \cdot\ \mathbf{n}, \qquad (5)$$

  where $\mathbf{v}$ is the velocity of the electrons in the CMB rest frame. See for example Rephaeli (1995) and Chluba & Mannheim (2002) for more details on the physics of the tSZ and kSZ effects.

Providing that the peculiar (group) velocity of clusters can me measured independently and subtracted, the kSZ effect would produce a dipole on the plane of the CMB detector as long as the intra-cluster gas rotates with a sufficient level of coherency** (as Fig. 3 suggests). The magnitude of the dipole (at the peaks) would be proportional to the number density of electrons times the integrated velocity of the gas along the line of sight. In Montero-Dorta et al. (2020a), we use the IllustrisTNG300 box to evaluate the performance of the kSZ effect as the cornerstone of an observational probe for halo spin bias. The details of the computation can be found in the aforementioned paper, I focus here on the main results of the analysis.

The goal of the study is to evaluate the "intrinsic signal", i.e., the amplitude of the signal in the absence of instrumental and observational uncertainties (see a similar approach in Baldi et al. 2018). Figure 4 shows, as an example, the tSZ and kSZ temperature-distorsion maps measured for a massive halo in IllustrisTNG300. The lower panel, in particular, shows the characteristic dipole pattern produced by the (velocity-subtracted) kSZ effect. The two lobes in different colors (+/− temperature distortions) represent the material that is, on average, moving away from and towards us, respectively.

The situation illustrated in Fig. 4 is common in the IllustrisTNG300 sample (50 000 halos with masses $11 < \log_{10}(M_{\rm vir}/h^{-1}M_\odot) \lesssim 14.5$). However, there are also many examples in which the internal motion of the gas is too chaotic for such a clear dipole to emerge. In order to evaluate the sample statistically, integrated tSZ and kSZ signals are conveniently measured for each map (represented by the quantities $Y_{\rm tSZ}$ and $S_{\rm kSZ}$, respectively). It is also convenient to define the ratio of signals $L_{\rm SZ} = S_{\rm kSZ}/Y_{\rm tSZ}$, which should be more directly related to the spin parameter (i.e., angular momentum per unit mass). See Montero-Dorta et al. (2020a) for more details.

The key to the performance of the SZ effect as an observational probe for spin bias lies in how well the integrated signals trace both halo mass and total halo spin. In Fig. 5, these relations are shown for the entire IllustrisTNG300 sample considered. The left-hand panel displays a good correlation between $Y_{\rm tSZ}$ and halo mass, particularly at the high-mass end. The correlation, although still significant, is weaker between our spin proxy $L_{\rm SZ}$ and total halo spin.

In the absence of any observational uncertainties, the above correlations are enough to allow for the recovery of the halo spin bias signal. This is demonstrated in Fig. 6 (left panel), where the secondary dependencies of halo clustering on the integrated SZ signals are displayed in the standard secondary-bias format. Halos with a higher value of $S_{\rm kSZ}$ and $L_{\rm SZ}$ are more tightly clustered than those with lower signals, with the mass trend following quite well that expected from spin bias. The right panel of Figure 6 indicates that these results remain qualitatively the same when halo mass is replaced by it tSZ proxy, $Y_{\rm tSZ}$.

Future ground-based instrumentation and space missions are expected to provide the spatial resolution and sensitivity required to measure the kSZ dipoles on an individual-object basis for sizeable cluster samples (see Mroczkowski et al. 2019 for a review). Some alternative routes towards an observational detection of spin bias that are worth citing include: SZ signal stacking, 21-cm emission of HI regions in galaxies, or (galaxy) spin-cosmic web alignments.

**This effect is sometimes called "rotational kSZ" (or rkSZ) in order to distinguish it from the case where the peculiar velocity is not subtracted.

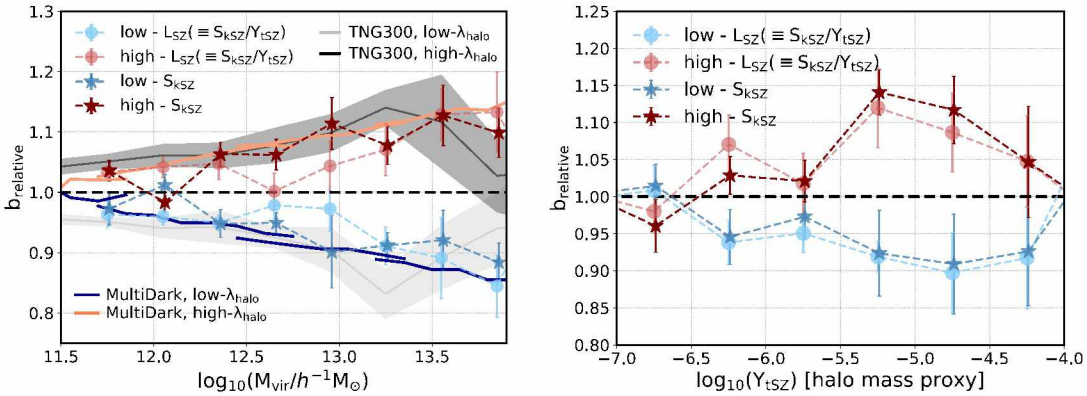

Figure 6: *Left panel:* Secondary dependence of halo bias on the integrated kSZ signal, S_{kSZ}, and the ratio of the integrated kSZ and tSZ signals, L_{SZ}, at fixed halo mass. In all cases, 50% halo subpopulations are employed to split the samples. Error bars on these measurements correspond to jackknife uncertainties. The SZ clustering results are compared with halo spin bias measurements from IllustrisTNG300 and MultiDark. The S_{kSZ} data points have been shifted slightly along the x-axis in order to make the error bars distinguishable. *Right panel:* Same measurement replacing halo mass by Y_{tSZ}.

5. Summary

Halo spin bias is a particular case of secondary bias in which halo spin is responsible for the secondary dependence of halo clustering at fixed mass. In this short paper, which summarizes my contribution to the 62 Meeting of the Argentinian Astronomical Society, I discuss the physical origins and observability of the effect, which has only been measured so far from N-body and hydrodynamical simulations. The main conclusions of our study, which is presented over several publications (Sato-Polito et al., 2019; Tucci et al., 2021; Montero-Dorta et al., 2020b,a), can be summarized as follows:

- At fixed halo mass, higher-spin halos from N-body numerical simulations have higher bias than their lower-spin counterparts above a characteristic redshift-dependent mass. The trend inverts below this characteristic mass.
- The inversion of the signal at the low-mass end is due to contamination from splashback halos, which are typically low-spin and low-mass halos that live in the vicinity of massive halos.
- At the high-mass end, the physical origins of the spin bias effect are still not fully understood. The connection with the surrounding tidal fields emerges as a promising theoretical route.
- It is also unclear to which extend this intrinsic spin bias signal is connected to other secondary bias trends such as assembly bias.
- IllustrisTNG300 predicts that both the total (stars, gas, DM) spin of central galaxies and that of the rotating intra-cluster gas correlate with halo spin. These links can be exploited in order to investigate the potential manifestation of halo spin bias on the galaxy population with observations.
- The SZ effect can be used in the future to probe the rotation of the intra-cluster gas and thus halo spin bias, once upcoming instrumentation achieves the spatial resolution and sensitivity required.

Acknowledgements: ADMD thanks Celeste Artale, Beatriz Tucci, Gabriela Sato-Polito, and Luis R. Abramo for their invaluable contributions to the results presented in this review. ADMD also thanks the organisers of the 62a Meeting of the AAA for their warm hospitality and FAPESP for financial support.

References

Baldi A.S., et al., 2018, MNRAS, 479, 4028
Barnes J., Efstathiou G., 1987, ApJ, 319, 575
Borzyszkowski M., et al., 2017, MNRAS, 469, 594–611
Bullock J.S., et al., 2001, ApJ, 555, 240
Chluba J., Mannheim K., 2002, A&A, 396, 419
Dalal N., et al., 2008, ApJ, 687, 12
Diemer B., 2020, arXiv e-prints, arXiv:2007.10992
Gao L., Springel V., White S.D.M., 2005, MNRAS, 363, L66
Gao L., White S.D.M., 2007, MNRAS, 377, L5
Heavens A., Peacock J., 1988, MNRAS, 232, 339
Johnson J.W., et al., 2019, MNRAS, 486, 1156
Klypin A.A., Trujillo-Gomez S., Primack J., 2011, ApJ, 740, 102
Lee C.T., et al., 2018, MNRAS, 481, 4038
Lin Y.T., et al., 2016, ApJ, 819, 119
Mansfield P., Kravtsov A.V., 2020, MNRAS, 493, 4763
Montero-Dorta A.D., et al., 2017, ApJL, 848, L2
Montero-Dorta A.D., et al., 2020a, arXiv e-prints, arXiv:2008.08607
Montero-Dorta A.D., et al., 2020b, MNRAS, 496, 1182
Mroczkowski T., et al., 2019, SSRv, 215, 17
Musso M., et al., 2018, MNRAS, 476, 4877
Peebles P.J.E., 1969, ApJ, 155, 393
Pillepich A., et al., 2018, MNRAS, 473, 4077
Press W.H., Schechter P., 1974, ApJ, 187, 425
Ramakrishnan S., et al., 2019, MNRAS, 489, 2977
Rephaeli Y., 1995, ARA&A, 33, 541
Salcedo A.N., et al., 2018, MNRAS, 475, 4411
Salcedo A.N., et al., 2020, arXiv e-prints, arXiv:2010.04176
Sato-Polito G., et al., 2019, MNRAS, 487, 1570
Sheth R.K., Tormen G., 1999, MNRAS, 308, 119
Sheth R.K., Tormen G., 2004, MNRAS, 350, 1385
Sunayama T., et al., 2016, MNRAS, 458, 1510
Sunyaev R.A., Zel'dovich Y.B., 1970, Ap&SS, 7, 20
Tucci B., et al., 2021, MNRAS, 500, 2777
Wechsler R.H., Tinker J.L., 2018, ARA&A, 56, 435
Wechsler R.H., et al., 2006, ApJ, 652, 71